Generation and optimization of electron currents along the walls of a conical target for fast ignition

S. Micheau, A. Debayle, E. d'Humières, J. J. Honrubia, B. Qiao et al.

Citation: Phys. Plasmas **17**, 122703 (2010); doi: 10.1063/1.3521571
View online: http://dx.doi.org/10.1063/1.3521571
View Table of Contents: http://pop.aip.org/resource/1/PHPAEN/v17/i12
Published by the American Institute of Physics.

Generation and optimization of electron currents along the walls of a conical target for fast ignition

S. Micheau,[1] A. Debayle,[2] E. d'Humières,[3] J. J. Honrubia,[2] B. Qiao,[1] M. Zepf,[1] M. Borghesi,[1] and M. Geissler[1]
[1]*Department of Physics and Astronomy, Queen's University Belfast, Belfast BT7 1NN, United Kingdom*
[2]*E.T.S.I Aeronáuticos, Universidad Politécnica de Madrid, 28040-Madrid, Spain*
[3]*Université de Bordeaux-CNRS-CEA, Centre Lasers Intenses et Applications, 33405 Talence, France*

(Received 19 July 2010; accepted 8 November 2010; published online 3 December 2010)

The interaction of an ultraintense laser pulse with a conical target is studied by means of numerical particle-in-cell simulations in the context of fast ignition. The divergence of the fast electron beam generated at the tip of the cone has been shown to be a crucial parameter for the efficient coupling of the ignition laser pulse to the precompressed fusion pellet. In this paper, we demonstrate that a focused hot electron beam is produced at the cone tip, provided that electron currents flowing along the surfaces of the cone sidewalls are efficiently generated. The influence of various interaction parameters over the formation of these wall currents is investigated. It is found that the strength of the electron flows is enhanced for high laser intensities, low density targets, and steep density gradients inside the cone. The hot electron energy distribution obeys a power law for energies of up to a few MeV, with the addition of a high-energy Maxwellian tail. © *2010 American Institute of Physics*. [doi:10.1063/1.3521571]

I. INTRODUCTION

Fast ignition[1,2] is an alternate scheme for inertial confinement fusion, in which an ultraintense laser pulse is used to generate hot electrons (or, alternatively, protons[3,4]), which subsequently ignite the precompressed fuel. This approach offers several advantages over central ignition,[5] but also suffers drawbacks due to propagation losses of the intense laser beam energy in the underdense coronal plasma. Recently, seminal experiments[6,7] have demonstrated that inserting a hollow cone in the spherical shell results in a significant enhancement of fusion events in the imploded target. Such promising results have thus motivated further experiments[8–12] and represent a milestone in the development of future equipments such as the High Power Laser Energy Research (HiPER) facility.[13]

However, the success of the fast ignition approach crucially depends on the efficient coupling of the ultraintense laser beam to the precompressed fusion pellet. This implies that fast electrons with appropriate energy are effectively generated and transported from the cone tip to the dense core.[5] Hybrid particle-in-cell (PIC) simulations[14–16] have demonstrated that self-generated resistive magnetic fields could collimate the relativistic electron beam during its transport through the coronal plasma, thus improving substantially the coupling efficiency. Nevertheless, these results have been shown to be highly sensitive to the initial properties of the fast electrons beam.[16]

Several experiments have been dealing with the electron generation in conical targets. Noticeable differences with respect to the planar geometry have been demonstrated in the number of electrons produced, their angular distribution,[17] and their energy distribution.[18] Cone-wire targets have further been developed to gain insight on both the generation and transport of hot electrons. The electron temperature measured shows a significant deviation[19] from the standard ponderomotive scaling.[20] However, the electron energy distribution strongly depends on whether the electrons are produced at the tip or on the sidewalls of the cone.[21] The major influence of the preplasma filling the cone and its potential prejudicial role have also been highlighted.[22,23] Thus, the experimental results obtained so far exhibit the peculiar response of cone targets to ultraintense laser light and further investigations are required to get a better understanding of the underlying physics and optimize the interaction parameters for future facilities.[24]

An important specificity of the laser-cone interaction is the potential formation of electron currents along the cone walls due to self-generated electromagnetic fields. Three-dimensional PIC simulations[25] have shown that electrons can be accelerated along the surface, thus producing a convergent hot electron flow toward the cone tip. These currents could also explain the enhanced energies observed in proton beams generated with cone targets.[26] However, the relevant parameters for the appearance of such currents remain elusive, since they have not been observed in recent simulations.[22] The formation of this focused fast electron beam is of paramount importance as the initial divergence of the relativistic electron beam has been shown to be a major limitation for fast ignition.[16]

In this paper, we investigate the characteristics of the electron flow emitted at the tip of a conical target irradiated by an ultraintense laser pulse. We present two-dimensional (2D) PIC simulations dedicated to the generation and optimization of a convergent fast electron beam toward the cone axis. We observe that surface currents along the cone walls can be efficiently produced for some given interaction parameters. The paper proceeds as follows: in Sec. II, we study the influence of the laser beam size with respect to the cone

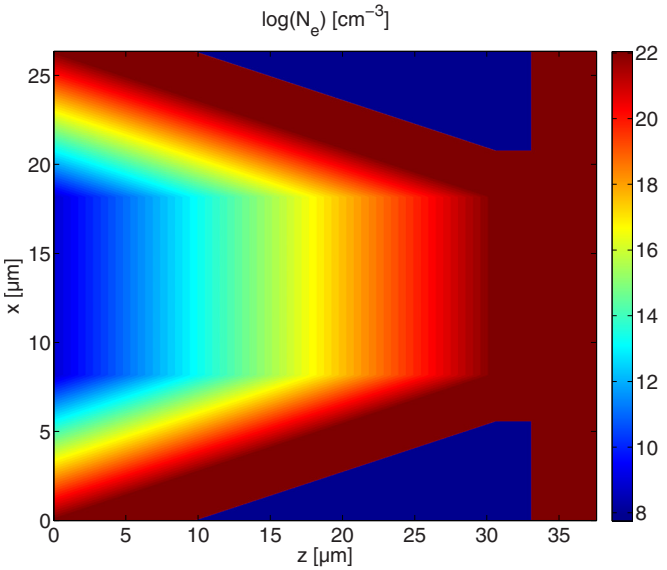

FIG. 1. (Color online) Initial density profile of the cone target (logarithmic scale).

tip size. We demonstrate that when the laser waist is larger than the cone tip extension, the guiding of electrons flows along the wall surfaces produces a convergent beam. Then, in Sec. III, we investigate the influence of the various interaction parameters on the wall currents in order to optimize the focusing effect of the cone.

II. FORMATION OF ELECTRON CURRENTS ALONG THE CONE WALLS

The simulations are performed with the fully relativistic PIC code ILLUMINATION (Refs. 27 and 28). The typical parameters used in this paper are the following: the simulation box is made of 2550×2048 cells with mesh sizes $\Delta z=\Delta x=0.016$ μm and the calculation time step is of 3.55×10^{-2} fs. The boundary conditions are absorbing for both electromagnetic fields and particles. The laser wavelength is $\lambda=1$ μm and its duration is set to 100 fs (FWHM). The temporal and spatial profiles are both Gaussian. The light is *p*-polarized as it is expected to maximize the surface currents.[29] *s*-polarization should, however, be considered in the future as experimental results are a mixture of those two cases. The target geometry is shown in Fig. 1. It consists of a 30° full-angle hollow cone, with 2.5 μm thick walls. The cone tip inner size is $d=10$ μm and its thickness is 2.5 μm. The target density is made of a collisionless plasma with immobile ions and its density is $10n_c$, where n_c denotes the critical density. We checked that using mobile Au^+ ions do not lead to any differences in the results obtained due to the short pulse duration employed in our simulations. The cone is filled with an exponentially decreasing preplasma, whose scale length is 1 and 0.25 μm in front of the cone tip and the walls, respectively, to ensure the density continuity. The electron population is simulated by 64 particles per cell. We use weighted particles so that we can simulate large density gradients without having to decrease the number of particles per cell in the low density regions. A dense plasma slab of 4.5 μm thick is placed behind the cone, which mimics the coronal plasma and limits the refluxing of electrons toward the inner part of the cone. There is no plasma behind the cone walls. Such targets have indeed been shown to enhance the number of electrons emitted toward the precompressed core.[30] In order to characterize the fast electron beam emitted at the cone tip, we follow the trajectories of about 8×10^6 quasiparticles, which initially belong to the cone or to the preplasma. At each time step, we extract the particles crossing the cone tip (at $z=30.6$ μm) with an energy threshold of 500 keV. Due to the electromagnetic fields building up at the cone tip (enhanced by the immobile ions) and the limited size of the coronal plasma, some particles are bounced back and forth across the cone tip. These particles crossing the surface several times are thus not considered. We checked that a larger coronal plasma (14.5 μm thick) gives similar results to the ones presented throughout this paper, the differences arising in the higher absolute value of the power law factor and the lower temperature of the electron energy spectra for the large coronal plasma case. This indicates that in the energy spectra presented here, the high-energy electron contribution is favored with respect to the low-energy electrons. Hence, the variations of the electron beam characteristics with respect to the various interactions parameters have to be considered rather than the actual values themselves.

It has to be noted that the pulse duration used throughout the paper is shorter than what is envisaged for fast ignition. However, our goal is not to simulate full-scale laser-cone interaction, but to understand the physics at stake and the relevant parameters for the generation of currents along the surfaces of the cone walls. Previous simulations[25] have shown that these currents can be formed in a few tens of femtoseconds.

We performed two sets of simulations. In the first case, the laser spot size is $w_{1/e}=3$ μm and is thus smaller than the cone tip inner size. In the second case, the spot size is 12 μm in order to investigate the contribution of the walls to the fast electron beam crossing the tip. The laser peak intensity is kept identical in both cases at $I_0=5.5\times10^{20}$ W/cm^2, which corresponds to a normalized vector potential of $a_0=20$. The temporal evolution of the number of electrons crossing the cone tip is shown in Fig. 2(a) for the two cases considered. When the laser spot size is smaller than the cone tip size, the time evolution of the electron yield follows the temporal profile of the laser pulse, with a duration of 95 fs (FWHM). When the laser spot size is larger than the tip size, there is a second component with a nearly constant yield which lasts for a few tens of femtoseconds after the end of the laser pulse. As shown in the next paragraph, this component is due to electrons flowing along the cone walls.

Figure 2(b) displays the electron energy flux crossing the cone tip as a function of the transversal coordinate, integrated over 500 fs. When $w_{1/e}$ is smaller than d, the spatial distribution resembles the Gaussian profile of the laser pulse, with a transverse size of 3.2 μm. On the other hand, when the laser pulse interacts with the cone walls, the spatial profile is mostly flat and its dimension matches the inner cone tip size. This supports previous findings suggesting that the fast electron beam extension is controlled by the cone tip

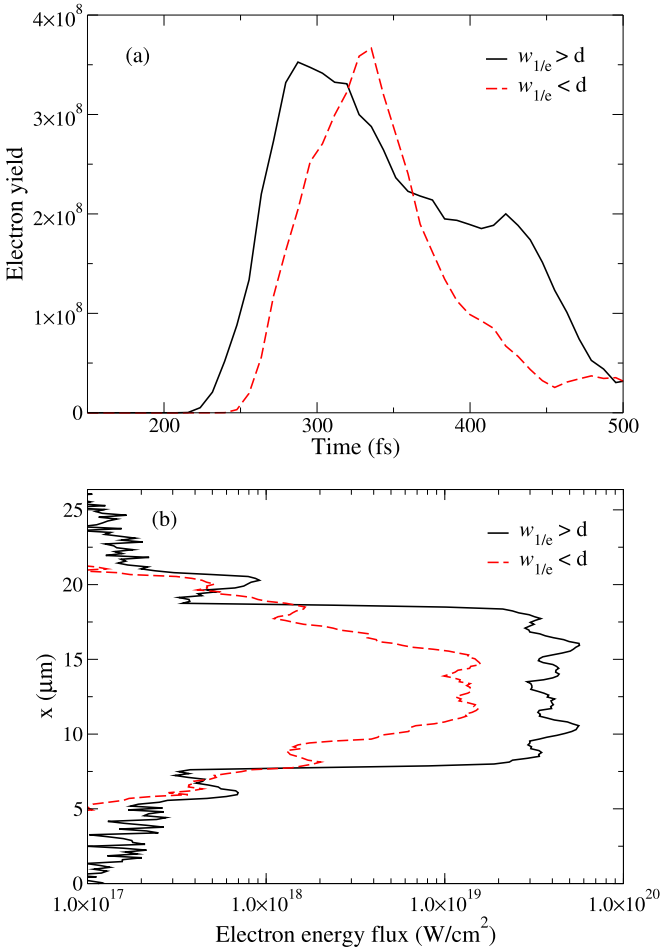

FIG. 2. (Color online) (a) Temporal evolution of the number of electrons crossing the cone tip when the laser spot size is larger than the cone tip size (solid line) and when the laser spot size is smaller than the cone tip size (dashed line). (b) Hot electron energy flux ($E>500$ keV) crossing the cone tip for the two cases.

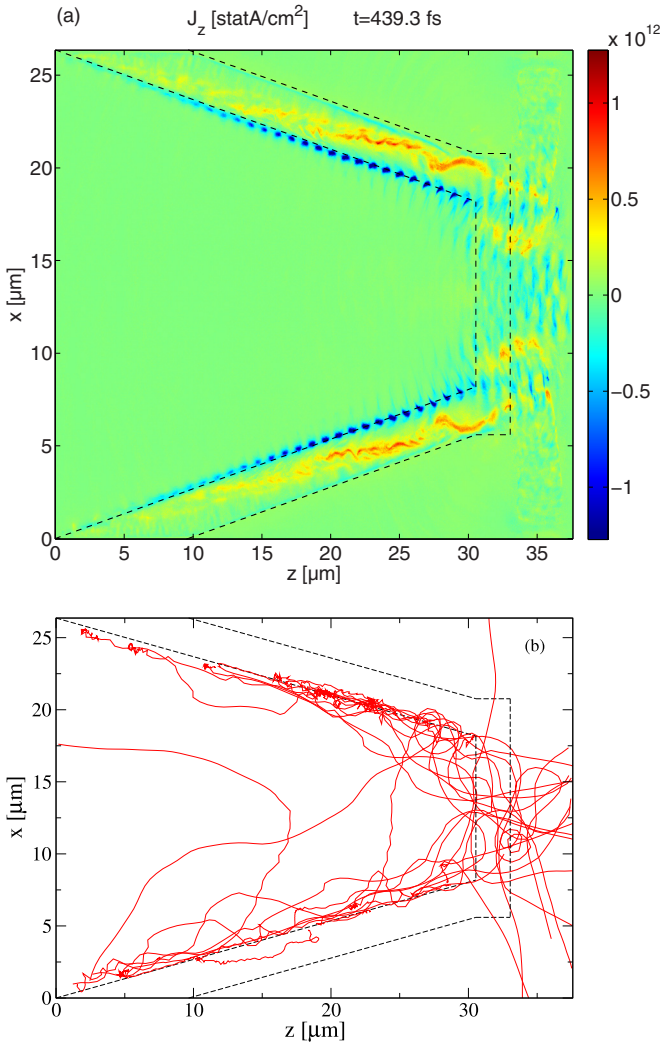

FIG. 3. (Color online) (a) Instantaneous longitudinal component of the electron current when $w_{1/e}>d$. (b) Typical electron trajectories obtained when $w_{1/e}>d$. The electrons are initially sampled 2 μm around the inner walls surfaces and their positions are recorded every 2 fs. In both figures, the dashed lines indicate the initial position of the cone.

size.[31] The total electron energy flux is 4.7 times higher for the larger laser beam size. Since the laser energy in 2D simulations scales as $I_0 w_{1/e}$, the conversion efficiency of the laser energy is thus slightly higher when the laser pulse interacts with the walls. Two peaks can be distinguished at $x=10.6$ and 15.6 μm in the spatial energy flux distribution when $w_{1/e}>d$. These contributions are due to electrons flowing along the inner surfaces of the cone walls. This can be seen in Fig. 3(a), where the instantaneous longitudinal component of the current at $t=439.3$ fs is shown, and in Fig. 3(b), which exhibits typical trajectories of electrons that are initially sampled around the inner walls surfaces. The laser pulse interacting obliquely with the cone sides generates electron currents along the walls, thus producing convergent electron flows toward the cone axis. The electron bunches are distributed regularly with $\lambda/\sin\theta$ intervals, where θ is the incident angle on the walls (75° in the present case). This is the signature of Brunel-type absorption mechanism.[32] It has been previously highlighted that the formation of a hot electron sheath along the surfaces do not necessarily imply that the hot electrons themselves are trapped inside this sheath.[22] However, here, the electron trajectories shown in Fig. 3(b) demonstrate the guiding effect of the walls surfaces. Since in Baton *et al.* the spot size was taken to be smaller than the cone tip size, the generation of these electron flows along the walls is attributed to the interaction of the laser pulse with the cone sidewalls.

Electron transport along the surface of foil targets have been observed for oblique incidence both experimentally[33,34] and theoretically.[35,36] When the laser incident angle is large (~70°), electrons can be trapped along the target surface in a potential well generated by self-induced quasistatic magnetic and electric fields.[37] As a result, in addition to an energy absorption rate of nearly 75%,[31] cones with an opening angle of 30° are optimal targets to favor the formation of currents on the surface of the sidewalls.

The energy spectrum of fast electrons emitted at the tip of a cone target is a crucial input parameter for hybrid codes to simulate the fast electron transport toward the precompressed target. It is generally chosen as a one-temperature Maxwellian distribution. Some numerical simulations have shown that the spectrum could be fitted by a

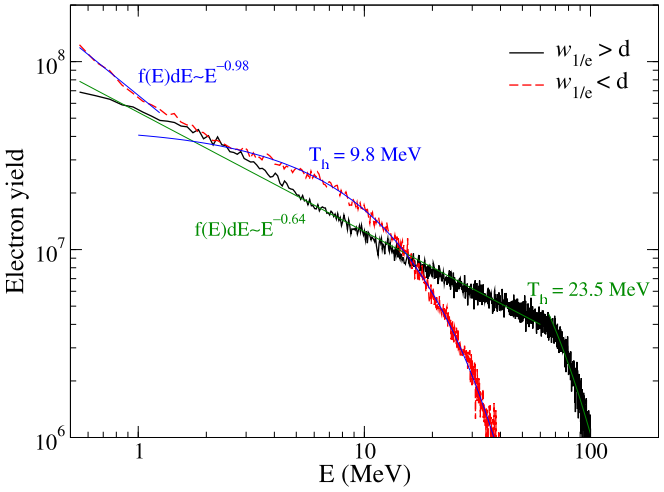

FIG. 4. (Color online) Time-integrated energy spectra of the electrons crossing the cone tip when the laser spot size is larger than the cone tip size (solid line) and when the laser spot size is smaller than the cone tip size (dashed line).

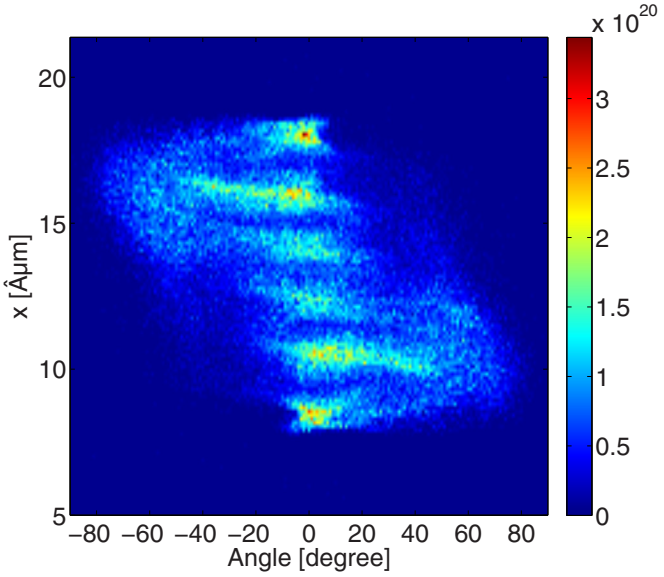

FIG. 5. (Color online) Distribution of the hot electron energy flux crossing the cone tip as a function of the transversal coordinate x and the direction of emission (with respect to the laser propagation direction) when $w_{1/e} > d$.

two-component[38] or three-component[39] Maxwellian distribution. However, a careful analysis of the various cone-generated spectra presented so far in the literature exhibits a more complex energy distribution function. In all our simulations, we find that the distribution function obeys a power law $f(E)dE \sim E^{-b}$ for electron energies of up to a few tens of MeV, where b varies with the interaction parameters. In addition to the power law component, the energy spectra are completed with a high-energy tail which is fitted by a Maxwellian distribution. Interestingly, a power law distribution function has been previously highlighted in Ref. 40 where the cone-attached target was described with a circular target in which a 60° wedge was removed.

The time-integrated energy spectra for the two laser spot sizes are shown in Fig. 4. Both spectra are fitted by a power law followed by a high-energy Maxwellian tail. However, for the smaller spot size, the power law extends up to 1.5 MeV, whereas it extends up to 80 MeV for the larger laser beam. The high-energy Maxwellian distribution for the narrow spot has a temperature of 9.8 MeV, which follows the usual ponderomotive law,[20] whereas the temperature for the wide beam is four times higher, indicating that the electrons are additionally accelerated with a different acceleration mechanism. The same effect has been observed experimentally when the laser pulse was focused on the cone walls rather than on the cone tip.[21] The higher temperature and the wider range of energies fitted by a power law in the case of the larger spot size are thus the results of the Brunel absorption and the subsequent surface acceleration on the sidewalls of the cone. Recent simulations demonstrated that electrons accelerated along a foil surface have a high-energy tail, which cannot be fitted by a Maxwellian distribution.[36] However, the power law dependence might not be due to the target geometry. Although further investigations are required, the spectrum obtained for the narrow spot size, as well as recently published results,[41] seems to indicate that a power law function up to a few MeV could also be observed for flat foil targets at these intensities.

The guiding of electrons along the walls generates a convergent fast electron beam toward the cone axis. In order to demonstrate the focusing effect of the cone, we present in Fig. 5 the map of the electron energy flux crossing the cone tip surface as a function of the direction of emission of the electrons (with respect to the laser propagation direction) and the transversal coordinate x. The pattern observed shows that electrons in the upper half of the figure (for $x > 13.3$ μm) have a predominantly negative direction of emission. This means that the particles generated in the upper part of the cone (i.e., the upper wall) are mainly going downward. On the other hand, in the lower half of the figure ($x < 13.3$ μm), the electrons have a positive angular distribution. Those electrons originating from the lower wall are thus essentially going upward. Consequently, both contributions are emitted toward the cone axis, leading to a converging electron beam. It is important to note that integrating over the whole spatial coordinate would give a large divergence angle, thus missing the converging effect of the cone.

III. INFLUENCE OF THE INTERACTION PARAMETERS OVER THE GENERATION OF ELECTRON SURFACE CURRENTS

The above simulations demonstrate the generation of electron surface currents on the walls of the cone. However, in some cases, no surface guiding effects have been reported for cone targets[22] or obliquely irradiated foils.[23] The formation of such electron flows thus depends on the interaction parameters.

A. Target density

The results presented in Sec. II, where $a_0 = 20$ and $n_e = 10 n_c$, are initially in the self-induced relativistic transparency regime.[42,43] However, at such high intensities, the preplasma gradient is dynamically compressed over short time

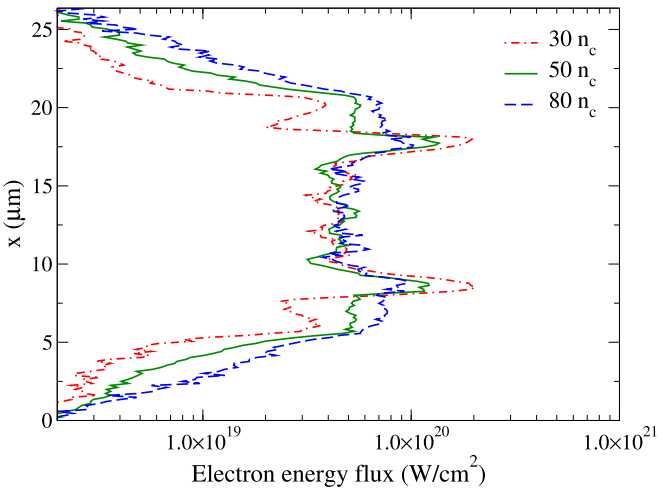

FIG. 6. (Color online) Hot electron energy flux ($E>500$ keV) crossing the cone tip for three target densities.

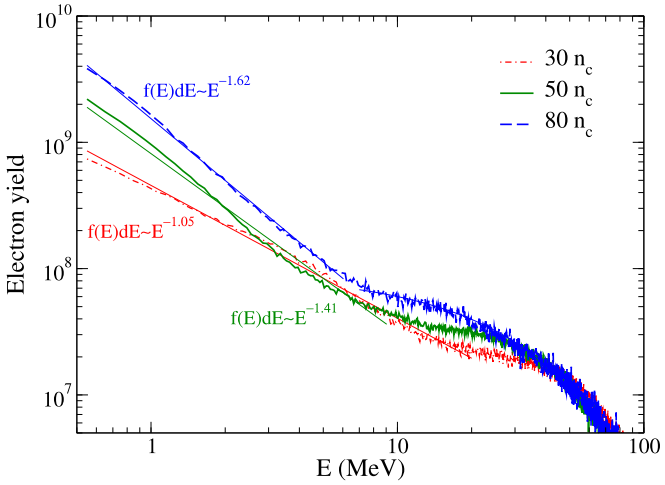

FIG. 7. (Color online) Time-integrated energy spectra of the hot electrons crossing the cone tip for three target densities.

scales, such that the main part of the laser pulse interacts with an overdense plasma.[44] In order to investigate the influence of the target density over the formation of electronic currents along the cone walls, we thus performed simulations with cone densities above γn_c, where $\gamma=(1+a_0^2)^{1/2}$ is the Lorentz factor of the electron in the laser field. To avoid the inherent changes in the profiles of the preplasmas, the cone targets were not initially filled with any particles. The influence of the preplasma scale length will be discussed in Sec. III D. The other interaction parameters remain identical to the ones used in Sec. II.

In Fig. 6, we show the transversal distributions of the electron energy flux crossing the cone tip for three cone densities above γn_c. The two peaks observed at $x=8.6$ μm and $x=17.9$ μm indicate the generation of electron currents along the cone walls in every cases. However, the strength of the currents decreases for larger target densities. More electrons are produced inside and behind the walls (for $x<8$ μm and $x>18.5$ μm) for higher densities, but those particles are not necessarily directed toward the cone axis and may not contribute to ignite the target. Thus, the relativistic transparency does not play a direct role in the formation of electron flows along the cone walls. However, the larger absorption of the laser energy for lower target densities[45,46] leads to stronger currents, hence favoring a focused fast electron beam toward the cone tip. In addition to the reduction of prejudicious collisional effects at the cone tip, the use of a low-Z material (such as CH) would thus be beneficial for fast ignition.[47]

The energy spectra of the fast electron beam are shown in Fig. 7 for the three target densities. In each case, the spectrum is fitted by a power law function followed by a high-energy Maxwellian tail. The power law component and its range of application vary with the density. The parameter b increases from 1.05 to 1.62 when n_e increases from $30n_c$ to $80n_c$. A rough fit of these values indicate a logarithmic increase of b with the density normalized to n_c. On the other hand, the extension $E_{\max}^{(\mathrm{pl})}$ of the power law distribution exponentially decreases when n_e increases, with $E_{\max}^{(\mathrm{pl})}=20$ MeV for $n_e/n_c=30$, $E_{\max}^{(\mathrm{pl})}=9$ MeV for $n_e/n_c=50$, and $E_{\max}^{(\mathrm{pl})}=6$ MeV for $n_e/n_c=80$. The high-energy cutoff is 80 MeV in every cases and is thus nearly independent of the cone density. However, the temperature of the Maxwellian distribution decreases when increasing the density, with $T_h=31$ MeV at $30n_c$, $T_h=25$ MeV at $50n_c$, and $T_h=23$ MeV at $80n_c$. The variation of the temperature with the target density was also demonstrated in Ref. 38, where an $n^{-1/2}$ dependence was found. Since hybrid simulations have shown that ignition is sensitive to the electron energy spectrum,[14,16] a more accurate consideration of the energy distribution in the fast electron transport codes is thus desirable for fast ignition.

B. Laser intensity

The laser pulse intensity is a preponderant parameter for fast ignition. 2D kinetic simulations[38] found a much lower electron temperature than the expected ponderomotive law[20] when a laser pulse with a spot size of 6 μm was focused on a 10 μm cone tip. However, recent experiments measured a temperature well above the usual $(I\lambda)^{1/2}$ scaling when the laser is focused on the sidewalls of the cone.[21]

Figure 8 presents the transversal distribution of the fast electron energy flux crossing the cone tip for three different laser intensities. The electronic density is set to $50n_c$ in every case and a preplasma with a scale length of 1 μm in front of the tip fills the cone. In the lower intensity case, the surface currents are almost negligible as the spatial distribution is nearly Gaussian. However, increasing the laser intensity results in a progressive enhancement of the currents strength. The contribution of the surface currents are clearly observed in the high-intensity case, at $x=10.5$ μm and $x=15.5$ μm, leading to a nearly flat electron energy flux distribution over the cone tip. Thus, for a fixed cone density, the strength of the surface currents is seen to increase when the laser intensity increases.

The enhancement of surface electron flows with the laser intensity has been observed experimentally when planar targets are irradiated obliquely.[33,34] It is attributed to the larger Brunel absorption efficiency, which varies as $I^{1/2}$.[48] It is in-

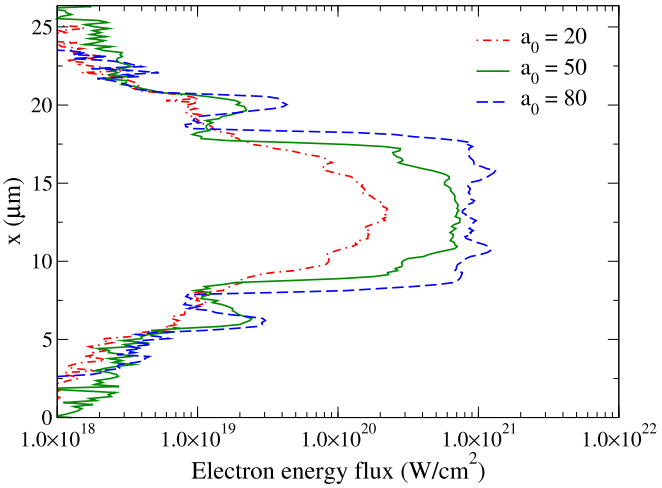

FIG. 8. (Color online) Hot electron energy flux (for $E>500$ keV) crossing the cone tip for three laser intensities.

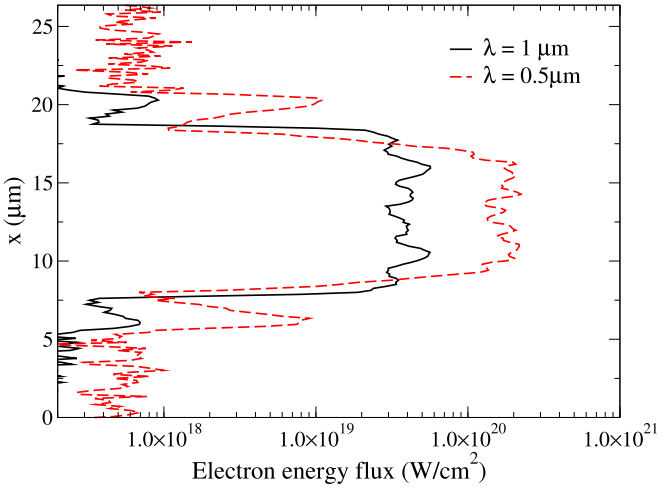

FIG. 10. (Color online) Hot electron energy flux crossing the cone tip (for $E>500$ keV) for two laser wavelengths.

teresting to note that a similar $I^{1/2}$ dependence of the surface electron temperature has been found in Ref. 35 for a tilted foil. In addition, the transversal energy flux distributions for the high intensities display two outer peaks at $x=6.2$ μm and $x=20.2$ μm. The strong sheath electric field which builds up at the cone/vacuum interface keeps the electrons from escaping the cone. Instead, they are reflected back and forth across the walls such that they move along the rear sides of the walls. They are finally emitted toward the cone axis and participate in the enhancement of the hot electrons yield.[30]

The energy spectra of the fast electron beam crossing the cone tip are shown in Fig. 9 for the three different intensities. The upper energy limit is fixed to 10 MeV as relativistic electrons beyond this maximum are ineffective for fast ignition.[16] Each distribution is fitted by a power law function followed by a Maxwellian high-energy tail (not shown). The energy range of the power law distribution, the Maxwellian temperature, and the high-energy cutoff increases with the laser intensity. A higher intensity leads to electrons with higher energies, resulting in a decrease of the power b, from $b=1$ for $I_0=5.5\times10^{20}$ W/cm^2 ($a_0=20$) to $b=0.74$ for $I_0=8.7\times10^{21}$ W/cm^2 ($a_0=80$). Although a proper scaling of the power law parameter's variation with the laser intensity requires a more detailed investigation, these results tend to indicate an exponential decrease of b with a_0.

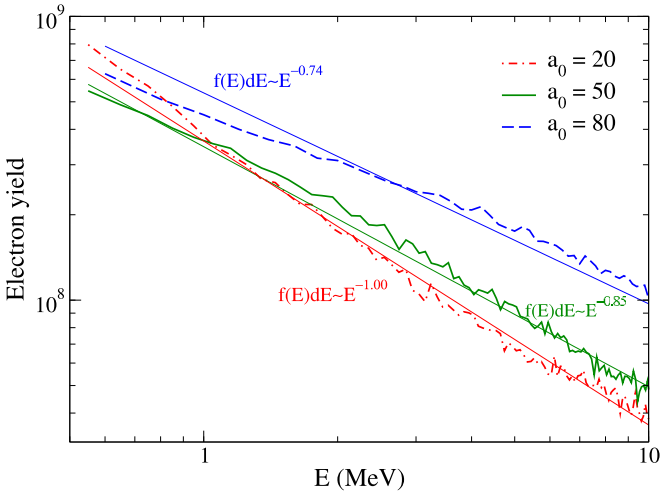

FIG. 9. (Color online) Time-integrated energy spectra of the hot electrons crossing the cone tip for two laser intensities.

C. Laser wavelength

The use of a shorter wavelength for the ignition pulse might be necessary if the penetration depth of the fast electron beam in the compressed fuel is larger than the optimal values obtained from target design studies,[49] i.e., if the hot electron average energy is too high when irradiating the cone with a 1 μm wavelength laser pulse. We thus performed simulations at ω and 2ω (here, ω refers to the fundamental frequency of a Nd:glass laser) in order to investigate the influence of the wavelength over the generation of wall currents and the fast electron beam energy distribution. The simulation at ω is the same as the one presented in Sec. II. The normalized laser intensity is kept identical in both cases ($a_0=20$), as well as the normalized target density, which is $10n_c$. The spatial distributions of the fast electron energy flux crossing the cone tip are shown in Fig. 10. Both distributions are nearly constant over the cone tip inner size. Thus, for a given ratio of a_0 over (n_e/n_c), the shorter wavelength gives a greater electron energy flux, which is nearly four times higher than at ω. The electron energy spectra, shown in Fig. 11, are fitted with a power law distribution function for energies between 500 keV and 10 MeV, with $f(E)dE\sim E^{-0.67}$ at ω and $f(E)dE\sim E^{-0.98}$ at 2ω. For the range of energies considered in the present case, the number of electrons is nearly four times higher at 2ω. This factor of 4 is related to the ponderomotive scaling but also to the fact that the actual value of the electronic density is twice higher in the 2ω case. As a consequence, the electrons with an energy of a few MeV (which are expected to maximize the coupling efficiency of the fast electron beam to the compressed core[24]) are favored for the shorter wavelength.

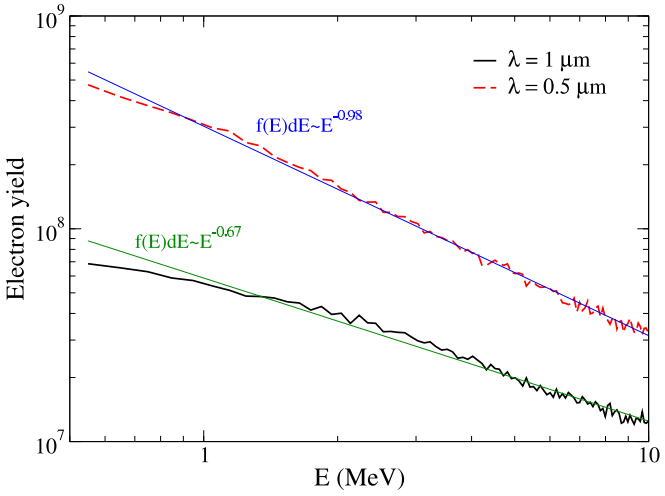

FIG. 11. (Color online) Time-integrated energy spectra of the hot electrons crossing the cone tip for two laser wavelengths.

D. Preplasma scale length

The unavoidable long-duration low-energy laser prepulse leads to the formation of a preplasma filling the cone. The induced density gradient consequently modifies the laser absorption fraction and the electron energy distribution.[46] As demonstrated in some experiments,[22,23] the presence of a large preplasma inside the cone can be a major drawback for the efficient generation of fast electrons. We present in Fig. 12 the hot electron energy flux crossing the cone tip for two preplasma scale lengths L_z and a void cone. The electronic density is set to $50n_c$ and the laser intensity is 5.5×10^{20} W/cm^2 in every cases. The plasma scale lengths given are in front of the cone tip and the lengths in front of the walls are accordingly adjusted to ensure the density continuity.

The void cone and the steeper gradient lead to a lower absorption efficiency of the laser energy along the cone axis with respect to the longer preplasma scale length, thus resulting in a lower energy flux emitted around $x=13.3$ μm. However, the wall currents' contributions (noticeable around $x=9$ μm and $x=17.5$ μm) are greatly increased, as well as the electrons generated inside and behind the cone walls (for $x<8$ μm and $x>18.5$ μm). This is a result of the larger Brunel absorption for steep gradients and/or steep interfaces. The strengths of the surface currents are identical for the $L_z=0.5$ μm and $L_z=0$ μm cases. After the rapid compression of the short preplasma,[44] the sharpened interface indeed resembles the steep wall. The surface currents are, however, generated closer to the cone axis in the presence of the short preplasma. This indicates that in this case, the absorption occurs at the steepened preplasma interface, while it occurs at the wall interface when there is no preplasma inside the cone. Noticing that the electrons generated inside and behind the walls are not necessarily emitted toward the cone axis and might not contribute to the ignition, these results indicate that a short preplasma scale length inside the cone remains acceptable for fast ignition, as long as it is steepened before the arrival of the main part of the pulse.

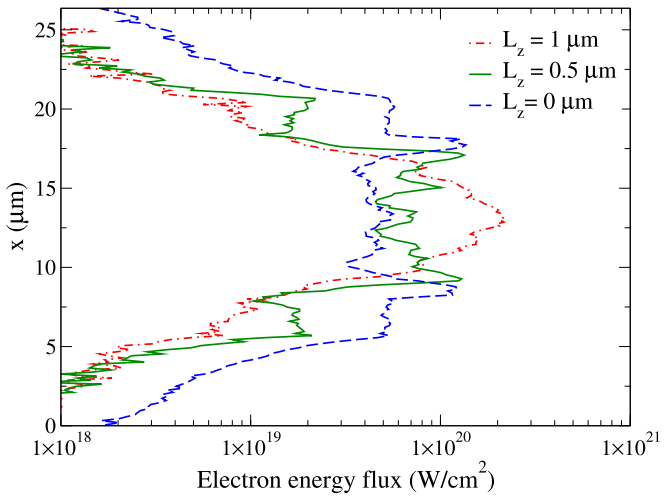

FIG. 12. (Color online) Hot electron energy flux (for $E>500$ keV) crossing the cone tip for three preplasma scale lengths. (scale lengths in front of the cone tip).

The preponderant effect of the preplasma and the enhancement of surface currents for steeper gradients have been experimentally demonstrated for plane targets obliquely irradiated.[33,34] These results are attributed to larger quasistatic electromagnetic fields developing on the target surface for a shorter plasma scale length, leading to the emission of electrons along the walls rather than in the specular direction.[34]

The electron energy spectra (not shown) are fitted by a power law for energies below 10 MeV. For the larger preplasma, b is equal to 1.10, whereas it increases to 1.20 for $L_z=0.5$ μm and 1.50 when there is no preplasma inside the cone. The steepening of the preplasma has indeed been shown to give lower energy electrons.[46,50,51]

E. Collisions

In order to get insight on the effect of collisions over the wall currents, we also carried out some simulations with mobile Au ions with a fixed ionization level of $Z=32$. These calculations were performed using the 2D collisional PICLS code.[52] The laser parameters are the same as the ones presented in Sec. II, with an intensity of 5.5×10^{20} W/cm^2, a duration of 100 fs, and a laser spot size of 12 μm. The simulation box is made of 2550×2048 cells with a cell size and a time step of $c\Delta t=\Delta x=\Delta z=\lambda/62$. Each cell contains 64 electrons and two ions with their numerical weights depending on the local density. The cone profile is the same as the one presented in Fig. 1 except that it is not filled with a preplasma. The density is set to $50n_c$ in the cone tip and the coronal plasma and is either $10n_c$ or $50n_c$ in the walls. For collisionless simulations, the electron temperature is fixed to $T_e=1$ keV. The boundaries are absorbing for the fields. The particles hitting the boundaries are reflected with a thermal temperature. Without collisions, we observed similar results than the ones presented in Sec. II, i.e., the wall surface currents, are higher for the lower wall density.

We performed similar simulations with collisions. The electron temperature is set to 50 eV. At first, we set up the

collisions accordingly to the kinetic density of $10n_c$ and $50n_c$ in the cone walls. In these cases, we observed the same behavior as in the collisionless simulations. Hence, we increased the collisional density to mimic the real gold solid density at n_{Au} and $n_{Au}/5$, where the kinetic density is $50n_c$ and $10n_c$, respectively. The use of a different density for the calculation of the collision frequency and for the kinetic calculations has been explored in Sentoku *et al.*[52] In these highly collisional cases, the wall surface currents decrease. This is due to the high collisionality of the return currents situated in the walls. Indeed, the relativistic surface currents are confined as long as the return currents inside the wall maintain the current neutrality.[37] This condition is broken in the case of a high plasma collisionality, since the electrons of the return currents are heated and scattered by the background ions. This short study of the collisional effect suggests that the surface currents may be efficiently generated and confined if we consider a low density target, such as a foam or a material with low Z. Complementary simulations using a hybrid code could help to investigate more thoroughly the collisional effects.

IV. CONCLUSIONS

The fast electron beam emitted at the tip of a laser-irradiated cone is studied through 2D PIC simulations in the context of fast ignition. When the laser spot size is larger than the cone tip size, the interaction of the pulse with the cone walls is highly beneficial as the formation of electron currents guided along the wall surfaces results in a focused fast electron beam, which can remain collimated by self-generated magnetic fields, thus enhancing the number of particles transported toward the precompressed core. The generated hot electron beam spectra are nicely fitted by a power law function for electron energies of up to a few MeV, rather than a Maxwellian distribution function, due to the various acceleration mechanisms at stake.

The strength of the surface currents along the sidewalls is enhanced when the laser intensity increases or when the density decreases. Using a shorter wavelength for the ignition beam could be considered, as it lowers the electron average energy without lowering the surface currents strength. In any case, the laser contrast has to be maximized to limit the preplasma filling the cone. The collisions decrease the surface current generation and confinement. A low density material with a low Z should thus be considered for the wall composition.

Finally, the results presented here are limited to short pulse durations. Longer pulse simulations have thus to be performed to investigate the influence of the processes appearing over longer timescales, such as plasma steepening or the development of instabilities at the cone tip.

ACKNOWLEDGMENTS

This work was supported in the framework of the HiPER project. We are grateful for the use of computing resources provided by STFCs e-Science facility and HPC resources from GENCI-CINES (Grant No. 2010-56129). The authors would like to thank Yasuhiko Sentoku for usage of the code PICLS.

[1] M. Tabak, J. Hammer, M. Glinsky, W. L. Kruer, S. C. Wilks, J. Woodworth, E. M. Campbell, M. D. Perry, and R. J. Mason, Phys. Plasmas **1**, 1626 (1994).
[2] M. Tabak, D. S. Clark, S. P. Hatchett, M. H. Key, B. F. Lasinski, R. A. Snavely, S. C. Wilks, R. P. J. Town, R. Stephens, E. M. Campbell, R. Kodama, K. Mima, K. A. Tanaka, S. Atzeni, and R. Freeman, Phys. Plasmas **12**, 057305 (2005).
[3] M. Roth, T. E. Cowan, M. H. Key, S. P. Hatchett, C. Brown, W. Fountain, J. Johnson, D. M. Pennington, R. A. Snavely, S. C. Wilks, K. Yasuike, H. Ruhl, F. Pegoraro, S. V. Bulanov, E. M. Campbell, M. D. Perry, and H. Powell, Phys. Rev. Lett. **86**, 436 (2001).
[4] S. Atzeni, M. Temporal, and J. J. Honrubia, Nucl. Fusion **42**, L1 (2002).
[5] M. H. Key, Phys. Plasmas **14**, 055502 (2007).
[6] R. Kodama, P. A. Norreys, K. Mima, A. E. Dangor, R. G. Evans, H. Fujita, Y. Kitagawa, K. Krushelnick, T. Miyakoshi, N. Miyanaga, T. Norimatsu, S. J. Rose, T. Shozaki, K. Shigemori, A. Sunahara, M. Tampo, K. A. Tanaka, Y. Toyama, T. Yamanaka, and M. Zepf, Nature (London) **412**, 798 (2001).
[7] R. Kodama, H. Shiraga, K. Shigemori, Y. Toyama, S. Fujioka, H. Azechi, H. Fujita, H. Habara, T. Hall, Y. Izawa, T. Jitsuno, Y. Kitagawa, K. M. Krushelnick, K. L. Lancaster, K. Mima, K. Nagai, M. Nakai, H. Nishimura, T. Norimatsu, P. A. Norreys, S. Sakabe, K. A. Tanaka, A. Youssef, M. Zepf, and T. Yamanaka, Nature (London) **418**, 933 (2002).
[8] K. A. Tanaka, R. Kodama, K. Mima, Y. Kitagawa, H. Fujita, N. Miyanaga, K. Nagai, T. Norimatsu, T. Sato, Y. Sentoku, K. Shigemori, A. Sunahara, T. Shozaki, M. Tanpo, S. Tohyama, T. Yabuuchi, J. Zheng, T. Yamanaka, P. A. Norreys, R. Evans, M. Zepf, K. Krushelnic, A. Dangor, R. Stephens, S. Hatchett, M. Tabak, and R. Turner, Phys. Plasmas **10**, 1925 (2003).
[9] P. Norreys, K. L. Lancaster, C. D. Murphy, H. Habara, S. Karsch, R. J. Clarke, J. Collier, R. Heathcote, C. Hemandez-Gomez, S. Hawkes, D. Neely, M. H. R. Hutchinson, R. G. Evans, M. Borghesi, L. Romagnani, M. Zepf, K. Akli, J. A. King, B. Zhang, R. R. Freeman, A. J. MacKinnon, S. P. Hatchett, P. Patel, R. Snavely, M. H. Key, A. Nikroo, R. Stephens, C. Stoeckl, K. A. Tanaka, T. Norimatsu, Y. Toyama, and R. Kodama, Phys. Plasmas **11**, 2746 (2004).
[10] J. A. Delettrez, J. Myatt, P. B. Radha, C. Stoeckl, S. Skupsky, and D. D. Meyerhofer, Plasma Phys. Controlled Fusion **47**, B791 (2005).
[11] N. Miyanaga, H. Azechi, K. A. Tanaka, T. Kanabe, T. Jitsuno, Y. Fujimoto, R. Kodama, H. Shiraga, K. Kondo, K. Tsubakimoto, Y. Kitagawa, H. Fujita, S. Sakabe, H. Yoshida, K. Mima, T. Yamanaka, and Y. Yzawa, in *Inertial Fusion Sciences and Applications 2003*, edited by B. Hammel, D. D. Meyerhofer, J. Meyer-ter-Vehn, and H. Azechi (American Nuclear Society, Lagrange Park, 2004), p. 507.
[12] M. H. Key, J. C. Adam, K. U. Akli, M. Borghesi, M. H. Chen, R. G. Evans, R. R. Freeman, H. Habara, S. P. Hatchett, J. M. Hill, A. Heron, J. A. King, R. Kodama, K. L. Lancaster, A. J. MacKinnon, P. Patel, T. Phillips, L. Romagnani, R. A. Snavely, R. Stephens, C. Stoeckl, R. Town, Y. Toyama, B. Zhang, M. Zepf, and P. A. Norreys, Phys. Plasmas **15**, 022701 (2008).
[13] M. Dunne, Nature (London) **2**, 2 (2006).
[14] J. J. Honrubia and J. Meyer-ter-Vehn, Nucl. Fusion **46**, L25 (2006).
[15] A. A. Solodov, K. S. Anderson, R. Betti, V. Gotcheva, J. Myatt, J. A. Delettrez, S. Skupsky, W. Theobald, and C. Stoeckl, Phys. Plasmas **16**, 056309 (2009).
[16] J. J. Honrubia and J. Meyer-ter-Vehn, Plasma Phys. Controlled Fusion **51**, 014008 (2009).
[17] Z. L. Chen, R. Kodama, M. Nakatsutsumi, H. Nakamura, M. Tampo, K. A. Tanaka, Y. Toyama, T. Tsutsumi, and T. Yabuuchi, Phys. Rev. E **71**, 036403 (2005).
[18] M. Nakatsutsumi, R. Kodama, P. A. Norreys, S. Awano, H. Nakamura, T. Norimatsu, A. Ooya, M. Tampo, K. A. Tanaka, T. Tanimoto, T. Tsutsumi, and T. Yabuuchi, Phys. Plasmas **14**, 050701 (2007).
[19] J. A. King, K. U. Akli, R. R. Freeman, J. Green, S. P. Hatchett, D. Hey, P. Jamangi, M. H. Key, J. Koch, K. L. Lancaster, T. Ma, A. J. MacKinnon, A. MacPhee, P. A. Norreys, P. K. Patel, T. Phillips, R. B. Stephens, W. Theobald, R. P. J. Town, L. Van Woerkom, B. Zhang, and F. N. Beg, Phys. Plasmas **16**, 020701 (2009).
[20] S. C. Wilks, W. L. Kruer, M. Tabak, and A. B. Langdon, Phys. Rev. Lett. **69**, 1383 (1992).

[21]H. Nakamura, B. Chrisman, T. Tanimoto, M. Borghesi, K. Kondo, M. Nakatsutsumi, T. Norimatsu, M. Tampo, K. A. Tanaka, T. Yabuuchi, Y. Sentoku, and R. Kodama, Phys. Rev. Lett. **102**, 045009 (2009).
[22]S. D. Baton, M. Koenig, J. Fuchs, A. Benuzzi-Mounaix, P. Guillou, B. Loupias, T. Vinci, L. Gremillet, C. Rousseaux, M. Drouin, E. Lefebvre, F. Dorchies, C. Fourment, J. J. Santos, D. Batani, A. Morace, R. Redaelli, M. Nakatsutsumi, R. Kodama, A. Nishida, N. Ozaki, T. Norimatsu, Y. Aglitskiy, S. Atzeni, and A. Schiavi, Phys. Plasmas **15**, 042706 (2008).
[23]L. Van Woerkom, K. U. Akli, T. Bartal, F. N. Beg, S. Chawla, C. D. Chen, E. Chowdhury, R. R. Freeman, D. Hey, M. H. Key, J. A. King, A. Link, T. Ma, A. J. MacKinnon, A. G. MacPhee, D. Offermann, V. Ovchinnikov, P. K. Patel, D. W. Schumacher, R. B. Stephens, and Y. Y. Tsui, Phys. Plasmas **15**, 056304 (2008).
[24]S. Atzeni, A. Schiavi, J. J. Honrubia, X. Ribeyre, G. Schurtz, Ph. Nicolaï, M. Olazabal-Loumé, C. Bellei, R. G. Evans, and J. R. Davies, Phys. Plasmas **15**, 056311 (2008).
[25]Y. Sentoku, K. Mima, H. Ruhl, Y. Toyama, R. Kodama, and T. E. Cowan, Phys. Plasmas **11**, 3083 (2004).
[26]K. A. Flippo, E. dHumières, S. A. Gaillard, J. Rassuchine, D. C. Gautier, M. Schollmeier, F. Nürnberg, J. L. Kline, J. Adams, B. Albright, M. Bakeman, K. Harres, R. P. Johnson, G. Korgan, S. Letzring, S. Malekos, N. Renard-LeGalloudec, Y. Sentoku, T. Shimada, M. Roth, T. E. Cowan, J. C. Fernández, and B. M. Hegelich, Phys. Plasmas **15**, 056709 (2008).
[27]M. Geissler, J. Schreiber, and J. Meyer-ter-Vehn, New J. Phys. **8**, 186 (2006).
[28]M. Geissler, S. Rykovanov, J. Schreiber, J. Meyer-ter-Vehn, and G. D. Tsakiris, New J. Phys. **9**, 218 (2007).
[29]Z. Li, H. Daido, A. Fukumi, A. Sagisaka, K. Ogura, M. Nishiuchi, S. Orimo, Y. Hayashi, M. Mori, M. Kado, S. V. Bulanov, T. Zh. Esirkepov, Y. Oishi, T. Nayuki, T. Fujii, K. Nemoto, S. Nakamura, and A. Noda, Phys. Plasmas **13**, 043104 (2006).
[30]H. Cai, K. Mima, W. Zhou, T. Johzaki, H. Nagatomo, A. Sunahara, and R. J. Mason, Phys. Rev. Lett. **102**, 245001 (2009).
[31]T. Nakamura, H. Sakagami, T. Johzaki, H. Nagatomo, K. Mima, and J. Koga, Phys. Plasmas **14**, 103105 (2007).
[32]F. Brunel, Phys. Rev. Lett. **59**, 52 (1987).
[33]Y. T. Li, X. H. Yuan, M. H. Xu, Z. Y. Zheng, Z. M. Sheng, M. Chen, Y. Y. Ma, W. X. Liang, Q. Z. Yu, Y. Zhang, F. Liu, Z. H. Wang, Z. Y. Wei, W. Zhao, Z. Jin, and J. Zhang, Phys. Rev. Lett. **96**, 165003 (2006).
[34]H. Habara, K. Adumi, T. Yabuuchi, T. Nakamura, Z. L. Chen, M. Kashihara, R. Kodama, K. Kondo, G. R. Kumar, L. A. Lei, T. Matsuoka, K. Mima, and K. A. Tanaka, Phys. Rev. Lett. **97**, 095004 (2006).
[35]T. Nakamura, K. Mima, H. Sakagami, and T. Johzaki, Phys. Plasmas **14**, 053112 (2007).
[36]J. Psikal, V. T. Tikhonchuk, J. Limpouch, and O. Klimo, Phys. Plasmas **17**, 013102 (2010).
[37]T. Nakamura, S. Kato, H. Nagatomo, and K. Mima, Phys. Rev. Lett. **93**, 265002 (2004).
[38]B. Chrisman, Y. Sentoku, and A. J. Kemp, Phys. Plasmas **15**, 056309 (2008).
[39]T. Nakamura, K. Mima, H. Sakagami, T. Johzaki, and H. Nagatomo, Laser Part. Beams **26**, 207 (2008).
[40]C. Ren, M. Tzoufras, F. S. Tsung, W. B. Mori, S. Amorini, R. A. Fonseca, L. O. Silva, J. C. Adam, and A. Heron, Phys. Rev. Lett. **93**, 185004 (2004).
[41]H. Cai, K. Mima, A. Sunashara, T. Johzaki, H. Nagatomo, S. Zhu, and X. T. He, Phys. Plasmas **17**, 023106 (2010).
[42]P. Kaw and J. Dawson, Phys. Fluids **13**, 472 (1970).
[43]J. Fuchs, J. C. Adam, F. Amiranoff, S. Baton, P. Gallant, L. Gremillet, A. Héron, J. C. Kieffer, G. Laval, G. Malka, J. L. Miquel, P. Mora, H. Pépin, and C. Rousseaux, Phys. Rev. Lett. **80**, 2326 (1998).
[44]A. J. Kemp, Y. Sentoku, and M. Takab, Phys. Rev. E **79**, 066406 (2009).
[45]H. Ruhl, A. Macchi, P. Mulser, F. Cornolti, and S. Hain, Phys. Rev. Lett. **82**, 2095 (1999).
[46]E. Lefebvre and G. Bonnaud, Phys. Rev. Lett. **55**, 1011 (1997).
[47]T. Johzaki, Y. Sentoku, H. Nagatomo, H. Sakagami, Y. Nakao, and K. Mima, Plasma Phys. Controlled Fusion **51**, 014002 (2009).
[48]Y. Sentoku, W. Kruer, M. Matsuoka, and A. Pukhov, Fusion Sci. Technol. **49**, 278 (2006).
[49]S. Atzeni, A. Schiavi, and C. Bellei, Phys. Plasmas **14**, 052702 (2007).
[50]A. J. Kemp, Y. Sentoku, and M. Tabak, Phys. Rev. Lett. **101**, 075004 (2008).
[51]R. Mishra, Y. Sentoku, and A. J. Kemp, Phys. Plasmas **16**, 112704 (2009).
[52]Y. Sentoku and A. Kemp, J. Comput. Phys. **227**, 6846 (2008).